European Conference on Computational Fluid Dynamics
ECCOMAS CFD 2006
P. Wesseling, E. Oñate, J. Périaux (Eds)

NUMERICAL SIMULATION OF THE AERODYNAMIC FLOW FIELD AND RADIATED NOISE OF A TRANSONIC CAVITY

Renzo Arina*, Nicola Ceresola†

* Professor, Politecnico di Torino, Corso Duca degli Abruzzi 24, 10129 Torino, Italy
e-mail: renzo.arina@polito.it

† Principal Research Engineer, Alenia Aeronautica, Corso Marche 41, 10146 Torino, Italy
e-mail: nceresola@aeronautica.alenia.it

Key words: Fluid Dynamics, Aeroacoustics, Turbulent Flows, Cavity Flows

Abstract. *A numerical simulation of the turbulent flow field of a transonic cavity and its associated far-field sound radiation, are presented. The test case is based on the experimental case M219 of QinetiQ. Two different turbulent simulations are performed, the first one is a URANS simulation with a k-w-EARSM turbulence model. while a DES turbulence model is employed in the second one. Comparisons with the experimental data show a good agreement for the lower frequencies in the case of the URANS simulations, while a better agreement in representing the small scale vortex structures is obtained with the DES model.*
The acoustic far-field radiation is obtained solving the convected wave equation, assuming as boundary conditions the wall pressure fluctuations computed with the DES model. The computed far-field noise directivity shows the existence of a directivity effect of the acoustic radiation, has expected in the case of cavity noise.

1 INTRODUCTION

The ability of reliably predicting the fluid-mechanic and aero-acoustic behaviour of cavity flows is nowadays of key importance in the design of weapon bays for modern military aircraft. Cavities on aerodynamic surfaces (weapon bay, landing gear bay, etc.) can generate both steady and unsteady perturbations in the surrounding flow field. Alteration of the static pressure distribution inside the cavity can result in large pressure gradient and unsteady flow which can generate self-sustaining oscillations which in turn can generate acoustic tones (resonance phenomena) arising from the cavity. The mechanism that leads to the creation of acoustic tones for an open cavity flow field consists of a coupling between instabilities in the shear layer that bridges the cavity and pressure waves produced in the cavity by the shear layer impingement on the rear cavity wall.

Acoustic tones appear at discrete frequencies that are linked to given pressure patterns inside the cavity. As far as the values of the resonance frequencies are concerned, a semi-empirical equation for their estimation, defined by Rossiter[1], has shown appreciable agreement with experimental values. Following the modified Rossiter formula, the frequency f associated with mode m is given as:

$$St_m = \frac{f_m L}{U_\infty} = \frac{m-\alpha}{\frac{M_\infty}{\sqrt{1+\frac{\gamma-1}{2}M_\infty^2}}+\frac{1}{k}} \tag{1}$$

where St is the Strouhal number, L is the cavity length, k= 0.57, α=0.062*L/D and D is the cavity depth .

So far no semi-empirical method is able to provide good agreement with experimental data for the estimation of tone amplitudes. A direct CFD simulation of sound sources is carried out in this paper, and compared with experimental data. On the other hand, to overcome the difficulties linked with the direct simulation of sound propagation, the aerodynamic calculation is separated from the noise propagation problem. The technique can be viewed as a postprocessor to the aerodynamic solution, allowing flexibility in the applications and requiring limited computational resources.

2 GEOMETRY AND FLOW PARAMETERS

The test case considered in this paper is based on an experiment conducted by QinetiQ[2]. An open cavity is contained in a flat plate of length 1,829 mm and width 431.8 mm, which is mounted in a transonic wind tunnel. The rectangular cavity has dimensions of L = 508 mm in length, D = 101.6 mm in depth and W = 101.6 mm in width, giving a ratio of L : D : W = 5 : 1 : 1. The experiment was performed with free stream conditions of M_∞ = 0.85, P_∞ = 6.21 × 104Pa, T_∞ =266.53K and Re = 13.47 × 10^6 per meter.

The cavity rig model used in the QinetiQ experiment is shown in Figure 1.

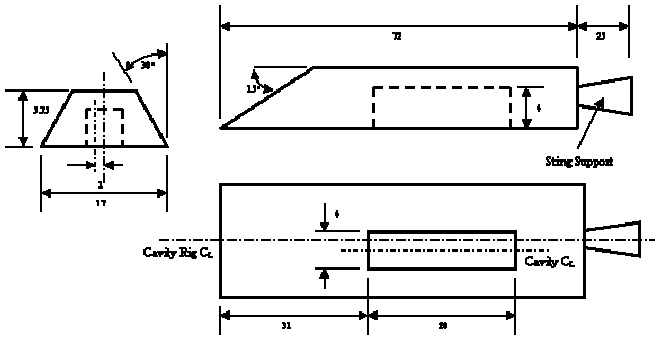

Figure 1 – Cavity rig model (dimensions in inches)

3 CFD MODEL

3.1 The code UNS3D

The computations have been performed using the code UNS3D. The solution algorithm is

based on a finite volume, node centred approach operating on an hybrid unstructured grid. The artificial dissipation model is derived from the nonlinear scheme of Jameson, with no eigenvalue blending.

The Navier-Stokes equations are integrated in time with a second order backward difference and dual time stepping. A five stage Runge-Kutta scheme is used to drive toward zero the residual at each time step. With the use of residual averaging, a local CFL number of 4.9 could be employed in the multistage sub iteration process.

The Weiss and Smith version of low Mach number preconditioning is implemented in the code. A sensor depending on cell Reynolds number was also introduced to avoid applying the preconditioning inside boundary layers. For the computation of the present test case, its application was found to be beneficial in order to reduce numerical dissipation and enhance convergence in low-Mach number pockets.

3.2 URANS turbulence model

A k-ω turbulence model was employed, that has been developed by Hellsten[3]. The model constants have been calibrated requiring consistent behaviour near boundaries between turbulent and laminar flow, inside shear flows and for zero pressure gradient wall flows. In particular, the calibration have been considered taking into account a variable c_μ , as it is the case if an algebraic stress model (EARSM) is included.

The Wallin-Johansson Explicit Algebraic Stress Model[4] (WJ-EARSM) is implemented using Hellsten's k-ω as the basis RANS model. The model is an exact solution of the corresponding ARSM in two-dimensional mean flow. In three dimensions there still is a complete, while approximate, solution.

The full anisotropic version of the model is used, i.e. the anisotropic part of the Reynolds stress tensor is directly introduced in the momentum equations, while the isotropic part is taken into account in the form of an effective variable c_μ..

3.3 DES turbulence model

The DES methodology essentially consist into using URANS as a subgrid scale model for LES in the regions where the grid resolution is sufficiently fine[5]. The DES length scale is therefore defined to be the minimum between the characteristic URANS length scale and a length related to the local grid, times an appropriate scaling coefficient:

$$l_{DES} = \min\{l_{RANS}, C_{DES}\Delta\} \tag{2}$$

where

$$l_{RANS} = k^{1/2}/(C_\mu \omega) \qquad\qquad l_{LES} = C_{DES}\Delta$$

and Δ can be the maximum distance between a cell vertex and the surrounding ones, $\Delta_i = \max_j\{l_{ij}\}$. In the case where very high aspect ratio cells are present in the LES region, it may be better to take the square root of the maximum surface between the cell faces,

$\Delta_i = \sqrt{\max_j \{S_{ij}\}}$. C_{DES} is an adjustable constant, depending on the RANS model used and on its particular numerical implementation. In the present case, C_{DES} is derived analytically imposing identity between the eddy viscosities given by the present SGS model and the Smagorinsky model in equilibrium ($P^k = D^k$, $P^\omega = D^\omega$) conditions. It is given by

$$C_{DES} = \frac{C_{SMAG}\left\{F\left(\frac{\gamma_1}{\beta_1 c_\mu}\right)^{0.75} + (1-F)\left(\frac{\gamma_2}{\beta_2 c_\mu}\right)^{0.75}\right\}}{1-F} \tag{3}$$

where C_{SMAG} is the Smagorinsky constant, γ_1, γ_2 are k-ω constants and F is the Menter blending function, to be used as a "shield" to prevent the LES model switching on inside boundary layers.

The switch between RANS and LES was implemented expressing the kinetic energy dissipation in the k-equation in the following form:

$$\varepsilon = \rho k^{3/2} / \min\{l_{RANS}, l_{LES}\} \tag{4}$$

The modified length scale is also employed in the constitutive relations, to obtain the time scale τ used in the computation of eddy viscosity and also to normalize the vorticity and strain rate tensors. We have therefore $\mu = c_\mu \rho k \tau$, where c_μ is a function of the scalar invariants of $\tau S_{ij}, \tau \Omega_{ij}$, and

$$\tau = \frac{\min(l_{RANS}, l_{DES})}{k^{\frac{1}{2}}} \tag{5}$$

It is worth to note that by this formulation, in LES regions the SGS model reduces effectively to a one-equation model.

4 ACOUSTICS PROPAGATION MODEL

The propagation and radiation in a medium with mean irrotational velocity field is governed by the convected wave equation which, in the case of a parallel mean shear flow with Mach number M, and cartesian coordinates, reads[6]

$$\left(\frac{\partial}{\partial t} + M\frac{\partial}{\partial x}\right)^2 p' - \left(\frac{\partial^2}{\partial x^2} + \frac{\partial}{\partial y^2}\right) p' = \bar{Q}_{ac}$$

with $M = U / c_0$, and the variables are made non dimensional with respect to a reference speed of sound c_0 and the cavity depth D as reference length. The term $\bar{Q}_{ac}$ contains the

source terms. The non-dimensional variable p' represents the acoustic fluctuations propagating with speed of sound c_0. Assuming that the pressure fluctuations have a harmonic time dependence

$$p' = \hat{p}(x, y)e^{iKt}$$

with $i = \sqrt{-1}$, $K = \omega D / c_0$ is the non-dimensional wave number or Helmholtz number, and ω the angular frequency, the convected wave equation transforms in

$$-\left[(1-M)\frac{\partial^2}{\partial x^2} + \frac{\partial^2}{\partial y^2}\right]\hat{p} + 2iKM\frac{\partial \hat{p}}{\partial x} - K^2\hat{p} = \hat{Q}_{ac}$$

The acoustic pressure can be computed after the mean flow field Mach number M is specified. In this way the range of the wave number $K \in [0, K_{\max}]$ is evaluated. For each value of K it is necessary to solve the associated convected Helmholtz problem. The acoustic pressure field is recovered performing an inverse DFT. Along artificial boundaries, to avoid incoming spurious reflections, appropriate non-reflecting boundary conditions must be imposed in the form of the Sommerfeld radiation condition.

The Helmholtz problem is approximated by a Finite Element method. The Fourier coefficient $\hat{p}$ of the acoustic pressure is interpolated by the nodal values, and the Galerkin variational formulation results in a complex matrix equation. The resulting sparse linear system, for the real and imaginary parts of $\hat{p}$ are solved by an iterative method. We have applied the GMRES method with ILUT preconditioning, consisting of an ILU decomposition with threshold and diagonal compensation. The performances of this iterative method remain the same also for very high wave numbers K provided the grid is sufficiently refined to represent the solution oscillations.

5 RESULTS

5.1 CFD grid and parameters of the computation

For the Navier-Stokes computations, the cavity was considered to be mounted on a flat plate and the computational domain made of a parallelepiped. A hybrid grid was generated, starting from a wall surface triangulation made of about 25000 nodes and 50000 triangles. A wall proximity grid made of 25 prismatic layers and an external grid made of tetrahedrals have then been generated. The total number of points was about 700000, forming 1010000 prisms and 765000 tetrahedrals. A view of the surface grid is shown in Figure 2.

Inflow-outflow characteristic boundary conditions were imposed at the inlet, outlet and top surfaces, while symmetry was enforced on lateral walls.

The computation was made at a Mach number of 0.85 and a Reynolds number of 1.37 millions based on the cavity depth. A fixed time step $\Delta t = 3.61\ 10^{-5}$ sec was used, corresponding to 1/50 of the travel time of the cavity length at free stream speed. A CFL number of 3.5 was used for the dual time stepping computation, and 100 sub iterations were

required to attain a drop in residuals between 1 and 2 orders of magnitude.

The URANS simulation was carried out for 1500 time steps, corresponding to 5.4 10^{-2} sec, while collecting a significant sampling window with DES required 2500 steps, corresponding to 9 10^{-2} sec.

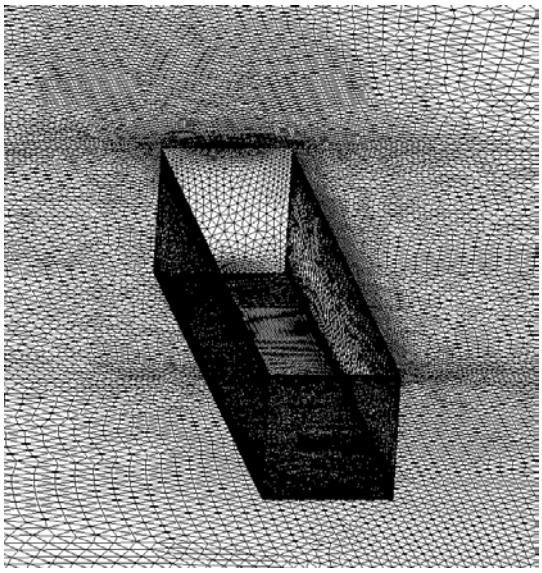

Figure 2 – Surface grid

5.2 Presures and sound pressure levels at cavity ceiling

Ten Kulite pressure probes were located at the cavity ceiling in the experiment, numbered from K20 to K29. In Figure 3 the time histories of ($P_{average}$ –P) at these locations are plotted, as they result from DES computations. From this plot one can appreciate how the amplitude of pressure oscillations regularly increases proceeding from the front to the rear edge of cavity.

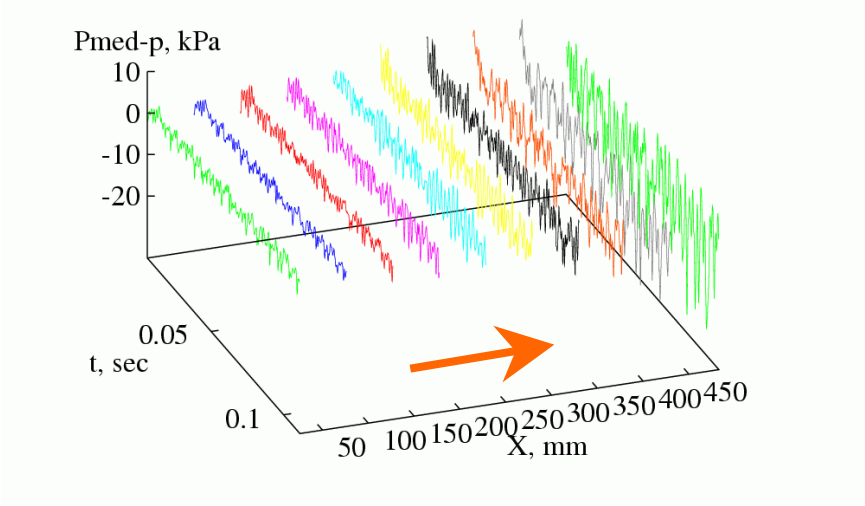

Figure 3 – Time histories of pressure at points K20-K29

A quantitative comparison with experimental data is then made at the locations of four of the pressure probes, located respectively near the front of the cavity (K20), near its centre (K23, K26) and near the exit edge(K29). Comparison is carried out in terms of spectral analysis of the Sound Pressure Level (SPL), a parameter in decibels (dB) derived from fluctuating pressure component and defined as follows:

$$SPL = 20\log\left(\frac{P_f}{2.9*10^{-9}}\right)$$

where P_f is the fluctuating component of the pressure.

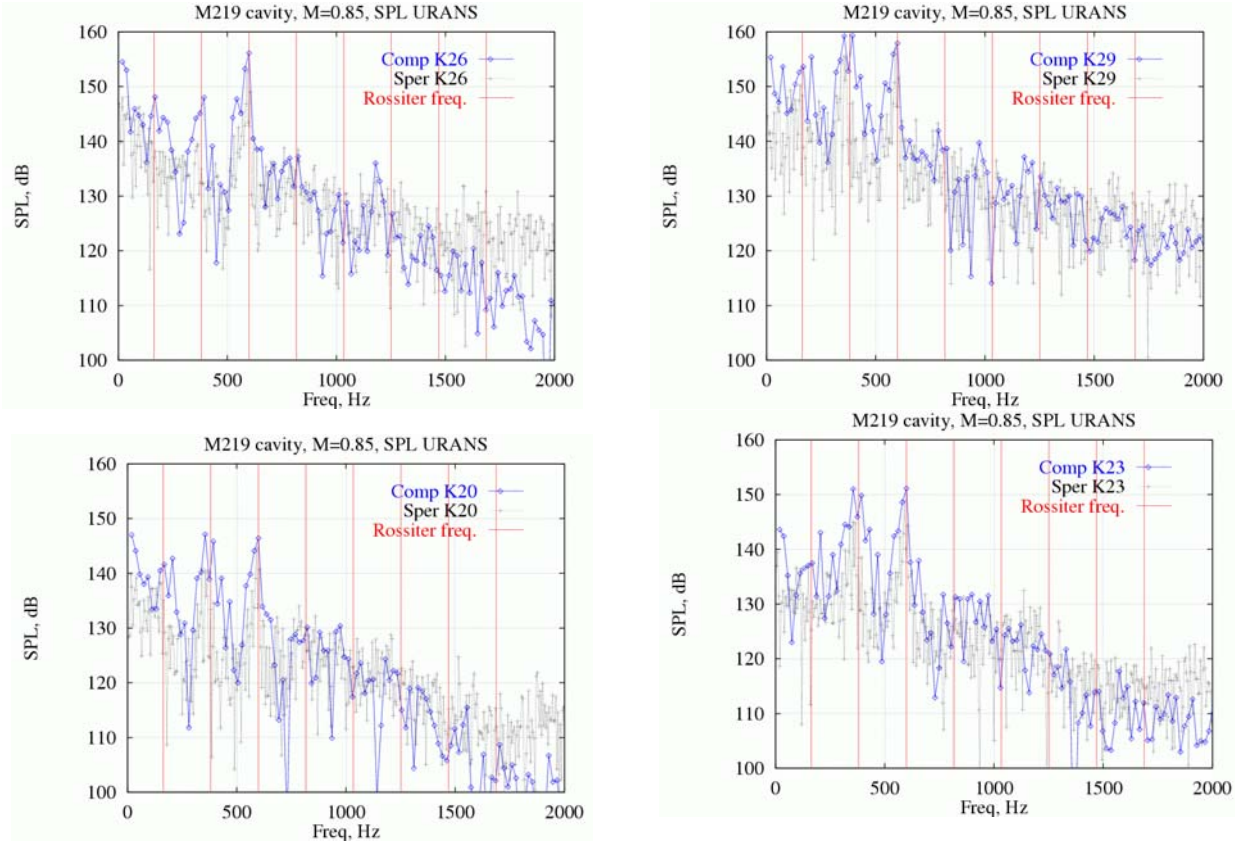

Figure 4 - SPL at four locations of cavity ceiling, URANS computation vs. experiment

In Figure 4 we can have a look at the sound pressure levels, in decibels, predicted with URANS and compared with the experimental data. The plots refer to the pressure points K20,K23,K26 and K29, located respectively near the inflow edge, near the centre of the cavity and near the exit edge. The vertical bars correspond to the Rossiter frequencies, as computed with the modified Rossiter formula. The magnitude of SPL up to 1000 Hz is

correctly predicted at least at first glance, and the first three resonance frequencies clearly result from the computed spectrum. As frequency increases, an more pronounced underprediction of sound levels is evidenced, possibly due to the numerical filtering made by the turbulence model. This interpretation is enforced when looking at SPL resulting from DES computation, in Figure 5 . Four to five Rossiter frequencies are shown in this case, while the richer and more complex spectrum is similar to that resulting from the experiment. Also more energy seems to be carried out at higher frequencies, coherently with the behaviour expected from the model.

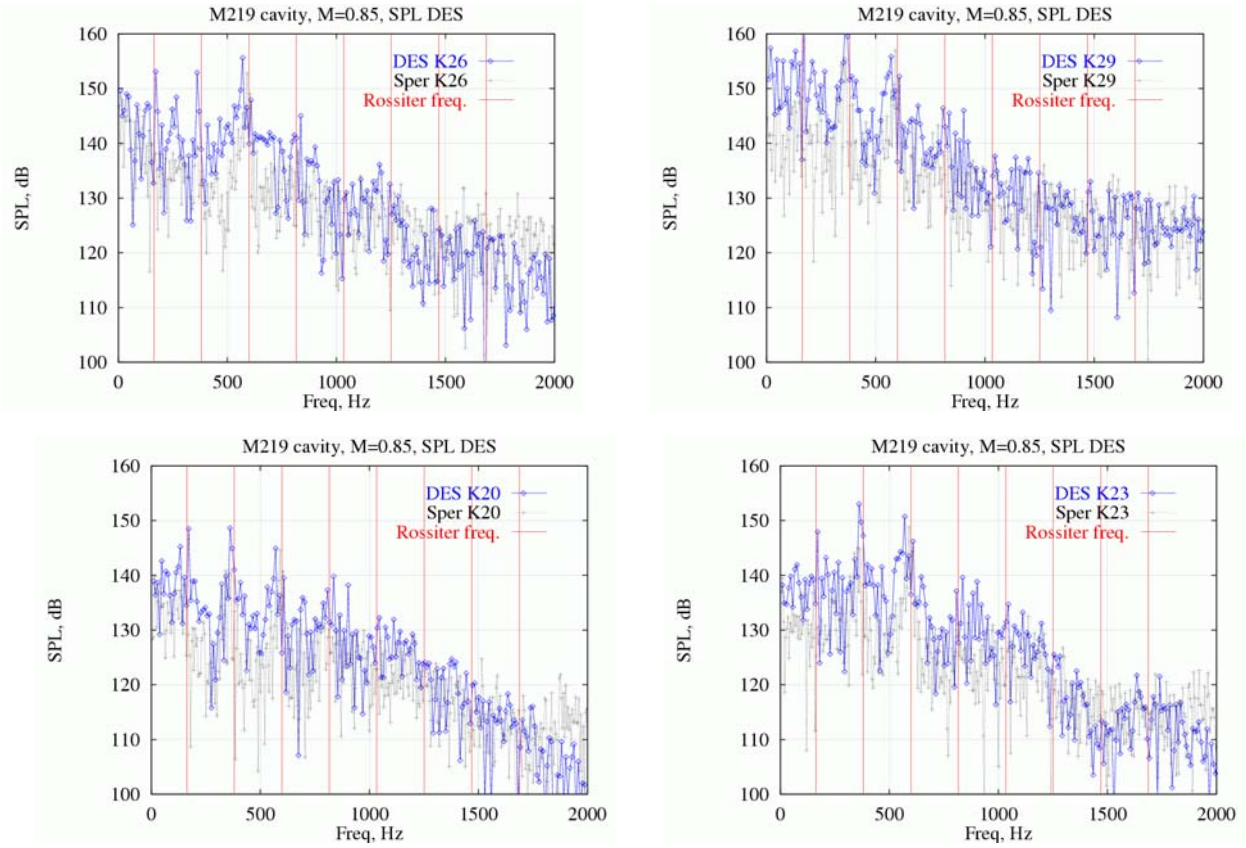

Figure 5 – SPL at four locations of cavity ceiling, DES computation vs. experiment

To qualitatively represent the difference between URANS and DES solutions, instantaneous iso-surfaces of total pressure loss are depicted in Figure 6 . The DES solution appears to be much richer in small scale vortex structures, which are not present in the URANS simulation.

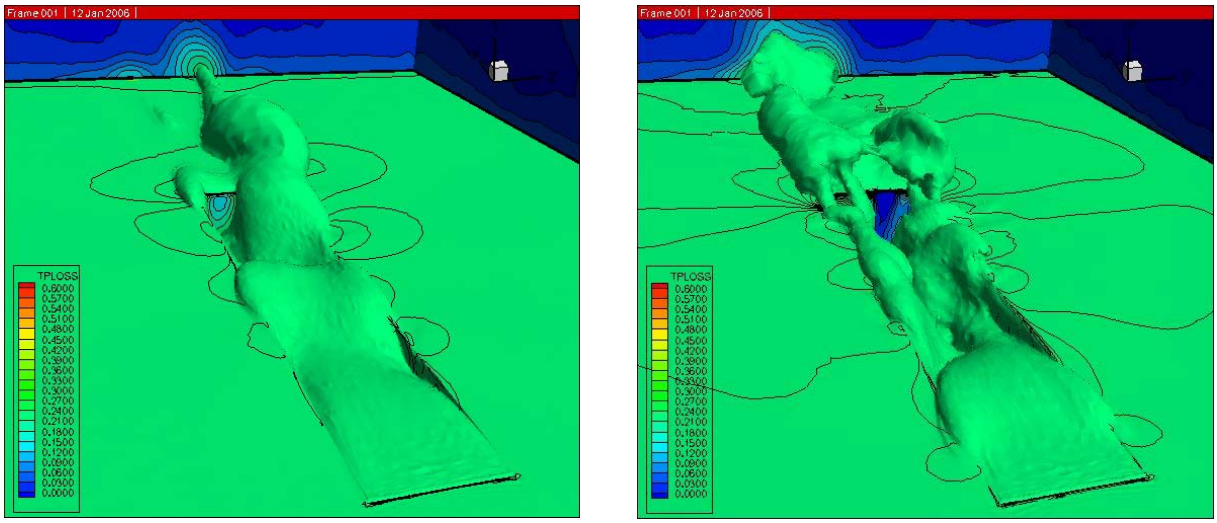

Figure 6 – Iso-surfaces of total pressure loss, URANS (left) and DES (right)

5.3 Far-field sound radiation

The two-dimensional sound radiation is performed on the vertical mid-plane ($z=0$). The convected wave equation is solved imposing as boundary conditions the fluctuating wall pressure computed with the DES simulation, along the flat plate and the cavity walls. No volume sources inside the domain, in the form of the Lighthill tensor, are taken into account. In this way the radiated acoustic field is only due to wall pressure fluctuations generated by the interaction of the vortical structures impinging on the walls. It is known that the major contribution to the cavity noise is due to this effect, which in the context of the acoustic analogy theory, is equivalent to a dipole source. The contribution to noise generation of the unsteady shear layer, the quadrupole source, is negligible.

This approximation greatly reduces the amount of data to be transferred from the flow solver to the acoustic solver. The wall pressure data are interpolated on the acoustic grid, which is coarser with respect to the computational grid employed for the turbulent flow simulation, along the walls. On the contrary, in the far field the acoustic grid must retain a smaller mesh size, compared with the fluid grid, in order to represent the acoustic waves, travelling for long distances without dissipation.

In the present computations, the unstructured grid, composed by triangle and quadrilaterals, has about 30000 nodes, and the circular far-field boundary, with origin in the mid of the boundary line separating the cavity from the external field, has a radius of ten times the cavity depth.

The mean flow field is assumed to be composed by a uniform flow, with M=0.85, outside the cavity, and fluid at rest inside the cavity. 64 samples, equally spaced in time, for a period $T=6.039\ 10^{-2}$ seconds, have been employed for describing the wall pressure fluctuations. The present amount of samples has been found to correctly represents the noise radiation

associated with the fundamental cavity modes. For representing the broadband noise, generated by the high frequency turbulent fluctuations, more samples should be employed.

In Figure 7 the Sound Pressure Level, in dB, with reference pressure 2×10^{-5} Pa, evaluated along a circle of ray $7.5D$ is shown. The directivity pattern is measured over the angular range of $0^0 \le \theta \le 180^0$. The mean flow incoming direction corresponding to $\theta = 180^0$. The levels range around 100 dB, with a peak radiation for θ around 130^0, showing the existence of a directivity effect of the acoustic radiation. This effect can be explained considering the instantaneous pressure patterns. As shown in Figure 8, the wave pattern clearly presents a strong directivity around the direction $\vartheta = 130^0$.

From the instantaneous pressure fields it can be seen that the highest peaks of wall pressure fluctuations are located in proximity of the downstream cavity corner. In this location the impinging shear layer, strongly interacts with the wall. Consequently the corner acts as a strong dipole source of noise, with a well defined directivity.

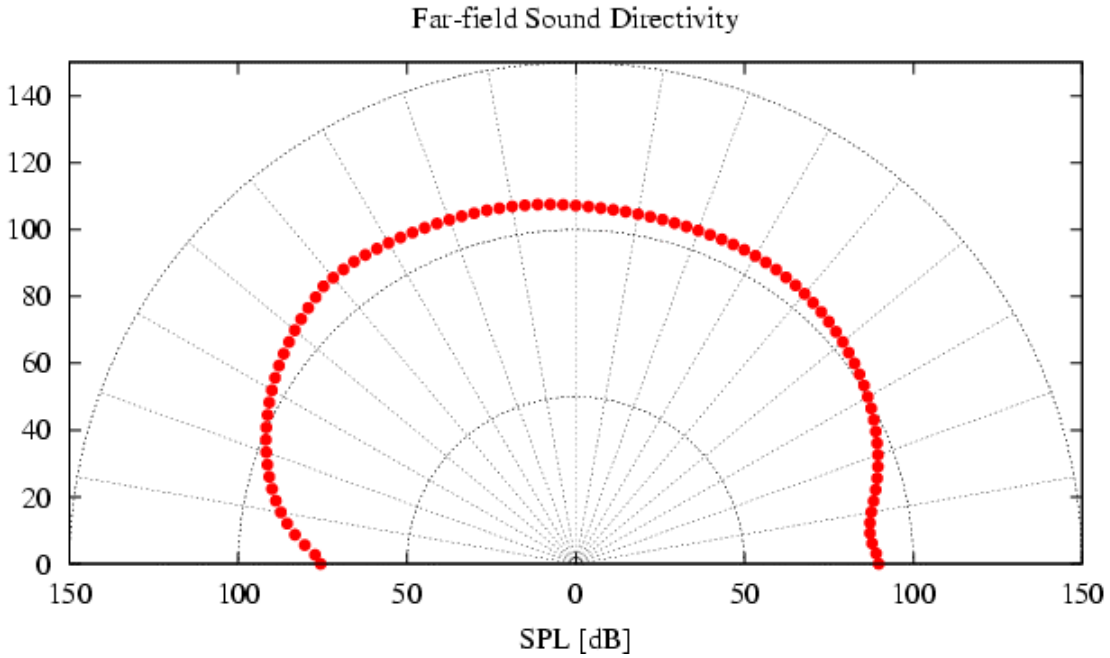

Figure 7 – Far-field sound directivity

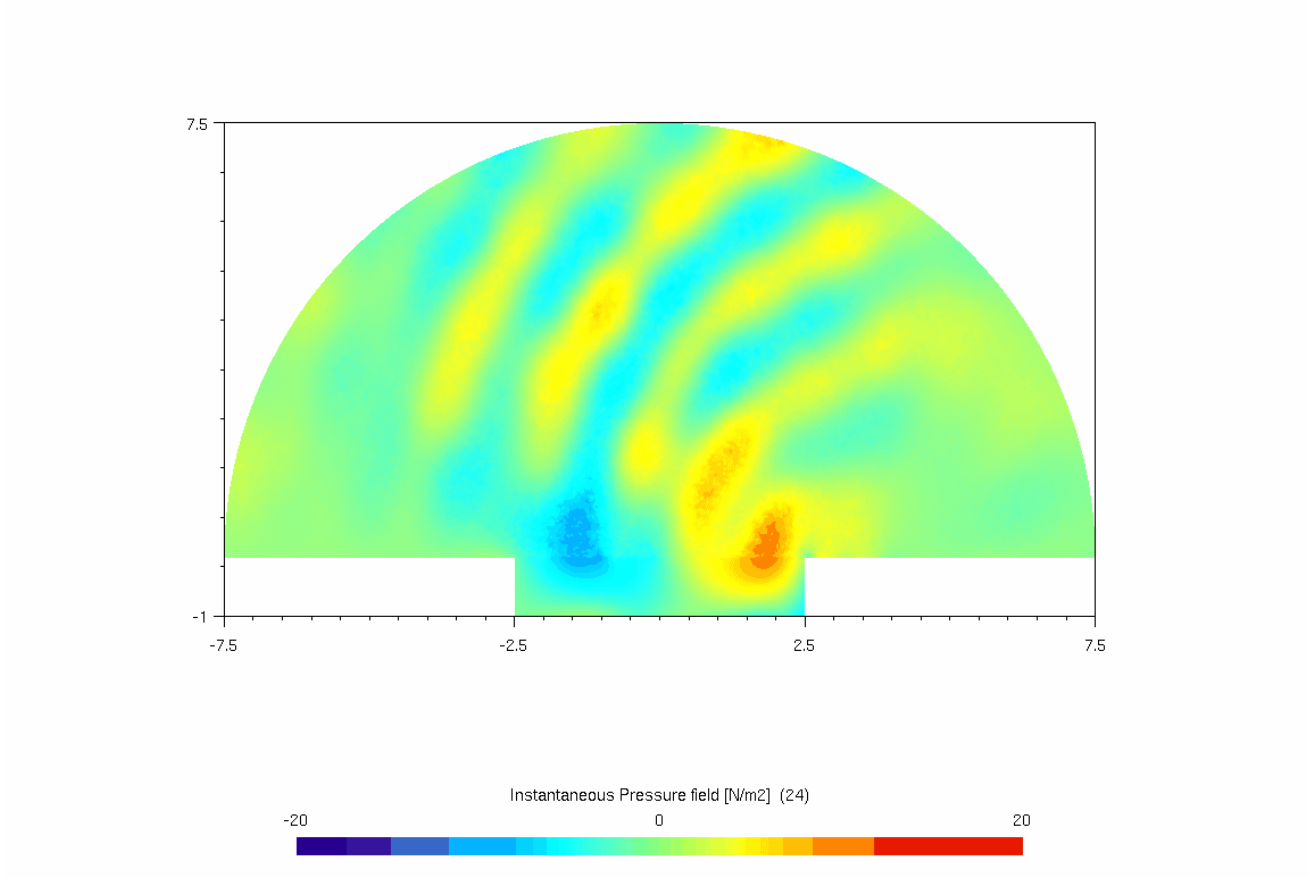

Figure 8 – Instantaneous acoustic pressure field

6 CONCLUSIONS

A numerical simulation of the turbulent flow field of a transonic cavity and its associated far-field sound radiation, have been presented. The geometrical and flow field conditions are based on the experimental test case M219 of QinetiQ. Two different turbulent simulations have been performed, a URANS simulation with a k-w-EARSM turbulence model. And a simulation with a DES turbulence model. Comparisons with the experiments show a good agreement for the lower frequencies in the case of the URANS simulations, while a better agreement in representing the small scale vortex structures is obtained with the DES model.

The two-dimensional acoustic far-field radiation is obtained solving the convected wave equation, assuming as boundary conditions the wall pressure fluctuations computed with the DES model. Even if the acoustic model neglects volume noise sources, the computed far-field directivity shows the existence of a directivity effect of the acoustic radiation, has expected in the case of cavity noise, for the strong interaction between the impinging shear layer and the downstream cavity corner.

7 ACKNOWLEDGEMENT

This work was undertaken, in part, within the DESider project (Detached Eddy Simulation

for Industrial Aerodynamics), a collaboration between Alenia, ANSYS–AEA, Chalmers University, CNRS–Lille, Dassault, DLR, EADS Military Aircraft, EUROCOPTER Germany, EDF, FOI–FFA, IMFT, Imperial College London, NLR, NTS, NUMECA, ONERA, TU Berlin, and UMIST. The project is funded by the European Community represented by the CEC, Research Directorate–General, in the 6th Framework Programme, under Contract No. AST3-CT-2003-502842.

REFERENCES

[1] J.E. Rossiter *"Wind tunnel experiment on the flow over rectangular cavities at subsonic and transonic speeds"* R. & M. N.3438, British Aeronautical Research Council, Oct. 1964

[2] M. J. de C.Henshaw. M219 cavity case. In *Verification and validation data for computational unsteady aerodynamics*, pages 453–472, Tech. Rep. RTO-TR-26, AC/323(AVT)TP/19, QinetiQ, UK, (2002)

[3] A. Hellsten, *"New Advanced k-ω Turbulence Model For High-Lift Aerodynamics"*, 42nd AIAA Aerospace Sciences Meeting and Exhibit, Reno, (2004)

[4] Wallin, S. & Johansson, A.V., *"An explicit algebraic Reynolds stress model for incompressible and compressible turbulent flows*", J. Fluid Mech. Vol. 403, pp. 89-132 (2000).

[5] M.Shur, M.Strelets, A. Travin, "*Detached Eddy Simulation (DES): General Description, Existing Versions, Constants Calibration, and Overview of Applications*", FLOMANIA Deliverable no.D4.41-5 , EEC Contract No. G4RD-CT-2001-00613 (2003)

[6] R. Arina, "*Numerical Prediction of Propagation and Radiation of Aft and Core Nozzle Noise*", 12th AIAA/CEAS Aeroacoustics Conference, Cambridge, Massachusetts, AIAA Paper 2006-2421 (2006).